

Gamma-ray and synchrotron emission from neutralino annihilation in the Large Magellanic Cloud

Argyro Tasitsiomi ^{a,c,1}, Jennifer Gaskins ^{b,c,2},
Angela V. Olinto ^{a,c,3}

^a*Department of Astronomy and Astrophysics, and*

^b*Department of Physics, and*

^c*Center for Cosmological Physics, The University of Chicago, Chicago IL 60637*

Abstract

We calculate the expected flux of γ -ray and radio emission from the LMC due to neutralino annihilation. Using rotation curve data to probe the density profile and assuming a minimum disk, we describe the dark matter halo of the LMC using models predicted by N-body simulations. We consider a range of density profiles including the NFW profile, a modified NFW profile proposed by Hayashi et al. (2003) to account for the effects of tidal stripping, and an isothermal sphere with a core. We find that the γ -ray flux expected from these models may be detectable by GLAST for a significant part of the neutralino parameter space. The prospects for existing and upcoming Atmospheric Cherenkov Telescopes (ACTs) are less optimistic, as unrealistically long exposures are required for detection. However, the effects of adiabatic compression due to the baryonic component may improve the chances for detection by ACTs. The maximum flux we predict is well below EGRET's measurements and thus EGRET does not constrain the parameter space. The expected synchrotron emission generally lies below the observed radio emission from the LMC in the frequency range of 19.7 to 8550 MHz. As long as $\langle\sigma v\rangle < 2 \times 10^{-26} \text{cm}^3 \text{s}^{-1}$ for a neutralino mass of 50 GeV, the observed radio emission is not primarily due to neutralinos and is consistent with the assumption that the main source is cosmic rays. We find that the predicted fluxes, obtained by integrating over the entire LMC, are not very strongly dependent on the inner slope of the halo profile, varying by less than an order of magnitude for the range of profiles we considered.

Key words: LMC, γ -rays, neutralino annihilation, EGRET, GLAST, ACTs

1 Introduction

Decades of observational evidence indicate that galaxies are surrounded by massive dark matter halos. It is also well-established that the baryon fraction of the universe is too small to account for the measured dark matter density. Most recent studies suggest that $\sim 23\%$ of the energy density of the universe is in the form of non-baryonic cold dark matter (CDM) (see, e.g., [1]).

Of the many candidate dark matter particles that have been proposed, the most popular is the Lightest Supersymmetric Particle (LSP). Strongly motivated by theoretical considerations, the LSP is stable in R-parity conserving models and has the appropriate relic density for masses $m_{LSP} \sim 100$ GeV (see, e.g., [2]). In Minimal Supersymmetric extensions of the Standard Model (MSSM), the LSP is most likely the lightest neutralino, χ [3]. Under certain assumptions, WMAP results favor $m_\chi < 500$ GeV [4], while accelerator experiments constrain $m_\chi \gtrsim 50$ GeV [5].

Neutralinos may be detected directly in low background experiments or indirectly by observations of their annihilation products. Products of $\chi\bar{\chi}$ annihilation rapidly decay into neutrinos and γ -rays, as well as electrons and positrons which emit synchrotron radiation in local magnetic fields. The rate of $\chi\bar{\chi}$ annihilation depends on the square of the neutralino number density. As such, the largest fluxes are expected to come from the densest regions. The galactic center is thus an obvious candidate for its density and proximity [6,7,8], but the numerous associated background signals might make it difficult to disentangle the neutralino annihilation flux.

High resolution N-body simulations of CDM halos find an abundance of substructure in galaxy-size halos. These studies predict that satellites of our galaxy, such as dwarf spheroidal galaxies, are embedded in dark matter halos of their own. In addition, these simulations find numerous dark “clumps”. The detection of neutralino annihilation products from these substructures may provide information about the clump density profiles as well as neutralino parameters. Previous studies have considered the annihilation signal from dwarf spheroidal galaxies [9,10,11] and dark matter clumps [12,13,14,15,16,17,18]. The detectability due to neutralino annihilation of other systems such as the LMC [19], M31 [20], and M87 [9], the globular cluster Palomar 13 [21], and galaxy clusters [22] have also been studied.

At a distance of 50.1 kpc [23], the LMC is an obvious choice for neutralino detection. There are several LMC mass estimates in the literature (e.g., [24,25,26,27,28,23]),

¹ iro@oddjob.uchicago.edu

² gaskins@oddjob.uchicago.edu

³ olinto@oddjob.uchicago.edu

and most agree within error bars. According to the most recent study, the mass of the LMC enclosed in a radius of 8.9 kpc is $M_{LMC} \simeq (8.7 \pm 4.3) \times 10^9 M_\odot$. To study neutralino annihilation it is important that the LMC be dark matter dominated. Van der Marel et al. [23] found that more than half of the LMC mass is in a dark halo. In addition, Sofue [27] argued that the LMC must have a dark and compact bulge with an anomalously high mass-to-light ratio $M/L \sim 20 - 50 M_\odot/L_\odot$.

The LMC has been observed in a wide range of frequencies, providing a wealth of data to draw upon. Past estimates of the LMC neutralino signal [19] focused solely on γ -rays and did not fit modern density profiles to the LMC halo. New rotation curve data and recent theoretical models of tidally stripped dark matter sub-halos motivate a new estimate of the LMC neutralino flux in γ -rays and in synchrotron emission. In addition, next-generation Atmospheric Cherenkov Telescopes (ACTs) and the upcoming GLAST satellite make this study of the LMC even more timely.

The flux of both γ -ray and synchrotron emission from neutralino annihilation in the LMC depends on the square of the density profile of the LMC dark halo. Thus, we begin the next section with a discussion of the structure of the LMC and describe fits of different dark matter profiles to the LMC rotation curve data. In §III we calculate the γ -ray flux and investigate the detectability prospects for ACTs and GLAST. In §IV we calculate the synchrotron flux and compare it to observations. We conclude in §V.

2 Modeling the LMC dark matter halo

Rotation curve data provides a dynamical measure of the mass distribution via

$$V_{rot}(r) = \sqrt{\frac{GM(r)}{r}}, \quad (1)$$

where $V_{rot}(r)$ is the rotation velocity at radius r and $M(r)$ is the total mass interior to r , $M(r) = \int_0^r \rho(r') d^3r'$. Given an observed rotation curve, we can study how well a particular model of the density distribution fits the observations. For the LMC rotation curve data, we use HI data from Kim et al. [26] that spans the range from 0.05 to 3.09 kpc with a velocity resolution of ~ 1.65 km/s, and carbon star data from Alves and Nelson [28] that covers a radius range of 4 to 8.2 kpc. We assume 8% error bars for the HI data given in [26].

Numerous N-body simulations have focused on understanding the structure of dark matter halos. Navarro, Frenk and White (NFW) [29,30] performed

N-body simulations of CDM halos and found that for a large range of masses the density profiles were well-described by the simple formula

$$\rho(r) = \frac{\rho_o}{(r/r_s)(1 + r/r_s)^2} , \quad (2)$$

with ρ_o and r_s a characteristic density and scale radius, respectively. The NFW profile can be alternatively characterized by r_s and the concentration parameter c which is related to ρ_o and is defined as the ratio r_v/r_s where r_v is the virial radius. The virial radius is defined as the radius within which a certain virial overdensity is reached, typically 180 times the average density of the universe. Behaving as r^{-1} at the center, the NFW profile is shallower than both the singular isothermal sphere and the Moore et al. [31] density profiles which behave at the center as r^{-2} and $r^{-1.5}$, respectively. Given the apparent discrepancy between the predictions of N-body simulations and observations (see, e.g., [32]), with the latter favoring shallow rather than very steep profiles at the center, we primarily focus on the NFW profile. This is a conservative assumption for CDM profiles since steeper density profiles lead to larger fluxes from neutralino annihilation. In particular, the effect of the baryonic component on the central density profile may increase the central density by more than an order of magnitude (see, e.g., [33]).

Hayashi et al. [34] performed N-body simulations to investigate how the density profile of an NFW halo changes due to tidal stripping. They found that the resulting profile can be described by a simple modification to the NFW profile:

$$\rho(r) = \frac{f_t}{1 + (r/r_{te})^3} \rho_{NFW} . \quad (3)$$

The factor f_t is a dimensionless measure of the reduction in central density while the “effective” tidal radius r_{te} describes the outer cutoff due to tides. The effect of tidal stripping on the initial NFW profile is to lower the characteristic density, to make it steeper in the outer region, and to introduce an outer cutoff. Since there is evidence that the LMC may be undergoing tidal disruption, we also model its halo using this profile.

As observations find that more than half of the mass within ~ 9 kpc of the LMC is dark [23], we assume that the disk is minimal (i.e., that the gravitational potential of the LMC is entirely due to dark matter) and search for the best fit NFW and Hayashi et al. profiles. For the NFW profile we find $r_s = 9.16$ kpc and $\rho_o = 1.66 \times 10^7 M_\odot/\text{kpc}^3$, corresponding to a concentration index $c \simeq 11.2$, and a χ^2 per degree of freedom of 1.01.

For the purposes of fitting the Hayashi et al. profile, we absorb the factor f_t into the NFW parameter ρ_0 and call the resulting parameter $\tilde{\rho}_0$. To distinguish between different models with almost identical χ^2 per degree of freedom values, we first fix the scale radius at the NFW best-fit value, $r_s = 9.16$ kpc. In this case, we find $r_{te} = 6.12$ kpc, $\tilde{\rho}_0 = 8.18 \times 10^6 M_\odot/\text{kpc}^3$ with a χ^2 per degree of freedom equal to 0.91.

Recent N-body simulations ([35], see also [34,36]) suggest that the process of tidal disruption of an NFW halo of mass comparable to the LMC may lead to a decrease in the scale radius of up to about 30%. The density profile of the LMC at the present is well-fitted by $r_s = 9.16$ kpc, so we can assume that this value represents a decrease of not more than 30% from the original value. Thus we can extrapolate that the scale radius of the original NFW halo that gave rise to the LMC was not more than ~ 13.1 kpc ($\simeq 9.16/0.7$ kpc $\simeq 1.4 \times 9.16$ kpc). To understand the effect that a larger scale radius has on the Hayashi et al. density profile and the resulting flux, we again fit the rotation curve data using a fixed $r_s = 13.1$ kpc. The resulting best-fit Hayashi et al. profile parameters are given by $r_{te} = 4.97$ kpc, $\tilde{\rho}_0 = 5.46 \times 10^6 M_\odot/\text{kpc}^3$ with a χ^2 per degree of freedom equal to 0.81.

All three fits to the rotation curve data are shown in Fig. 1. While all the fits are acceptable, the Hayashi et al. profiles better fit the data at the outer radii. The masses predicted by these models are in reasonable agreement with estimates in the literature – the Hayashi et al. gives a mass of $\sim 9 \times 10^9 M_\odot$ within 8.9 kpc, while the NFW fit gives $\sim 3 \times 10^{10} M_\odot$ within 8.9 kpc, slightly above the observationally determined $(8.7 \pm 4.3) \times 10^9 M_\odot$ within 8.9 kpc by [23].

The relatively small tidal radii of the Hayashi et al. fits deserve comment. Observations typically indicate the tidal radius for the LMC r_t is greater than about 10 kpc ([23] and references therein). However, different observational methods for determining this quantity may give significantly different values. While a precise determination of the tidal radius would require knowing the distance at which regular isopleths of a certain class of stars end, more practical estimators involve the Roche limit (valid for point masses), or the Jacobi limit (where the centrifugal force on the satellite is taken into account). For instance, the tidal radius determined via the Roche limit ($r_{tR} = (M_{LMC}/2M_{MW})^{1/3}d$) relies upon approximate mass estimates for both the Milky Way halo (M_{MW}) and the LMC. These methods do not directly correspond to the Hayashi et al. profile parameter r_{te} , which is an *effective* tidal radius. Careful inspection of the enclosed mass as a function of radius for tidally stripped objects in the Hayashi et al. study reveals that the mass does not necessarily reach a plateau at $r = r_{te}$, but continues to increase with radius (e.g., up to 2 times r_{te} , which is closer to the observational r_t). Consequently the parameter r_{te} does not necessarily correspond to the observationally determined tidal radius.

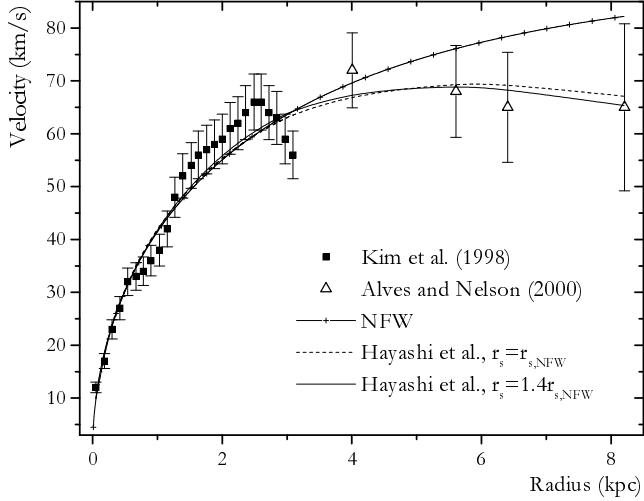


Fig. 1. Rotation curve of the LMC: square points from HI data [26] and triangle points from carbon star data [28]. The crossed curve is the NFW fit. The dashed curve is the Hayashi et al. fit obtained by fixing the scale radius to the best fit value found for the NFW profile. The solid line corresponds to the Hayashi et al. fit obtained by fixing the scale radius at $r_s \sim 1.4r_{s,NFW}$ to account for the possible evolution of r_s (see text for details).

Lastly, even if we force $r_{te} = 15$ kpc, we find that the Hayashi et al. fit becomes essentially the same as the NFW best fit (the Hayashi et al. best fit $r_s = 9.35$ kpc while the NFW best fit $r_s = 9.16$ kpc). This is not surprising given that with such a large r_{te} the difference between the Hayashi et al. and the NFW profiles arises at radii much larger than that for which there is rotation curve data available.

For completeness, we consider three additional profiles. We examine two recently proposed profiles: the Stoeckl et al. [37] profile which was found to accurately fit rotation velocity curves of satellite halos in some simulations, and the more centrally concentrated Moore et al. [31] profile. We also look at a shallower profile – an isothermal sphere with a core as derived in [28] by fitting the same rotation curve data we use here. Both the Moore et al. [31] and the Stoeckl et al. [37] profiles seem less favored by the rotation curve data – they give χ^2 values per degree of freedom 5.49 and 4.24 respectively. The isothermal sphere with a core represents a less ideal scenario. Instead of making the assumption of a minimum disk, the stellar disk and gas contributions are included in the model by Alves and Nelson [28]. In this case, the halo profile is given by

$$\rho(r) = \frac{\rho_o}{1 + (\frac{r}{a})^2} , \quad (4)$$

with $\rho_o = 10^8 M_\odot/\text{kpc}^3$ and core radius $a = 1$ kpc.

3 The γ -ray Emission

Neutralino annihilation proceeds through a number of channels, many of which produce γ -rays in the final state (see e.g., [8]). Here we consider only the continuum γ -ray emission due to the decay of neutral pions produced in hadronic jets.

$$\begin{aligned} \chi + \bar{\chi} &\rightarrow \pi^0 + X \\ &\hookrightarrow \pi^0 \rightarrow \gamma + \gamma. \end{aligned} \tag{5}$$

Given the uncertainties in the dark matter density distribution, a full calculation of the gamma-ray emission in the large dimensional parameter space of SUSY models is not warranted. Instead, we use the approximate Hill spectrum [38] based on the leading-log approximation (LLA). For MSSM models, this approximation is reasonable for neutralino masses below the W mass and above the top quark mass. Furthermore, the simplified spectra derived below vary from the fit obtained in [39] by no more than a factor of a few for neutralino masses from 10 GeV up to a few TeV.

Assuming that the hadronic jets contain only pions and that equal numbers of π^+ 's, π^- 's, and π^0 's are produced, the neutral pion spectrum is given approximately by

$$\frac{dN_{\pi^0}}{dx_\pi} \simeq \frac{5}{16} x_\pi^{-3/2} (1 - x_\pi)^2 \tag{6}$$

with $x_\pi = E_{\pi^0}/m_\chi$. Furthermore, the probability per unit energy that a neutral pion with energy E_{π^0} produces a photon with energy E_γ through the process shown in Eq. (5) is $2/E_{\pi^0}$. Thus, from Eq. (6) we get for the continuum photon spectrum,

$$\frac{dN_{cont.}}{dx_\gamma} \simeq \int_{x_\gamma}^1 \frac{2}{y} \frac{dN_{\pi^0}}{dy} dy \tag{7}$$

with $x_\gamma = E_\gamma/m_\chi$ and $y = E_{\pi^0}/m_\chi$. The number of continuum photons produced per annihilation through this channel with energy greater than a specified threshold is found by integrating this spectrum, which gives

$$N_{cont.}(E_\gamma \geq E_{th}) = \int_{x_{th}}^1 \frac{dN_{cont.}}{dx_\gamma} dx_\gamma \quad (8)$$

$$= \frac{5}{6}x_{th}^{3/2} - \frac{10}{3}x_{th} + 5\sqrt{x_{th}} + \frac{5}{6\sqrt{x_{th}}} - \frac{10}{3} \quad (9)$$

where $x_{th} = E_{th}/m_\chi$.

The γ -ray emission coefficient j is

$$j = N_\gamma(E \geq E_{th}) \frac{\langle \sigma v \rangle_\gamma}{m_\chi^2} \rho^2(r) , \quad (10)$$

where N_γ is the number of photons above the energy threshold as found in Eq. (8). The quantity $\langle \sigma v \rangle_\gamma$ is the thermally averaged cross section times velocity for annihilation into γ -rays, and $\rho(r)$ is the density profile of the halo. The specific intensity of γ -rays, $I(R)$, as a function of projected radius R , is given by

$$I(R) = \frac{1}{4\pi} 2 \int_0^{z_{max}(R)} j dz , \quad (11)$$

for which z is the coordinate along the line of sight and $z_{max}(R) = \sqrt{r_{max}^2 - R^2}$ where r_{max} is the radius of the object. The γ -ray flux F from an object at a distance d from us is given by

$$F = \frac{1}{2} \frac{1}{4\pi d^2} \int_0^{r_{max}} j d^3r . \quad (12)$$

The radial dependence of j is confined to $\rho^2(r)$. We isolate the dependence of the flux on the specific halo profile and distance to the LMC by defining K as

$$K = \frac{1}{2} \frac{1}{4\pi d^2} \int_0^{r_{max}} \rho^2(r) d^3r . \quad (13)$$

The γ -ray flux is then given by

$$F = K \frac{N_\gamma \langle \sigma v \rangle_\gamma}{m_\chi^2} . \quad (14)$$

For r_{max} we use 3.1 kpc, which is the radial extent of the LMC as observed in γ -rays by EGRET [40]. We take the distance to the LMC to be 50.1 kpc as

found in [23]. We give K in units of $(\text{GeV}/c^2)^2/\text{cm}^5$, which gives the flux F in $\text{cm}^{-2} \text{s}^{-1}$ with $\langle\sigma v\rangle_\gamma$ in $\text{cm}^3 \text{s}^{-1}$ and m_χ in GeV/c^2 .

For the NFW model $K = 3.65 \times 10^{19} (\text{GeV}/c^2)^2/\text{cm}^5$, while for the Hayashi et al. fits $K = (0.84 - 0.85) \times 10^{19} (\text{GeV}/c^2)^2/\text{cm}^5$ depending on the exact value of the scale radius. For the isothermal sphere with a core we obtain $K = 0.43 \times 10^{19} (\text{GeV}/c^2)^2/\text{cm}^5$. The more centrally concentrated Moore et al. and the Stoeckl et al. profiles give slightly higher fluxes, by factors $\sim 2-4$ with respect to the NFW case. Clearly, the small variations between the fluxes produced by these models are overwhelmed by observational uncertainties. Fits to all of these profiles give K on the order of $10^{19} (\text{GeV}/c^2)^2/\text{cm}^5$. These profiles behave similarly and consequently give similar fluxes, thus, for simplicity we focus on the NFW profile. The mild dependence on the halo profile, and more specifically on its central slope, is expected given that we calculate the flux from the entire observed extent of the LMC, rather than just from the innermost region. Thus, the flux depends most strongly on the “normalization” of the profile which is set by the mass enclosed in the volume over which we integrate.

EGRET detected a flux of $(14.4 \pm 4.7) \times 10^{-8}$ photons ($E > 100 \text{ MeV}$) $\text{cm}^{-2} \text{s}^{-1}$ from the LMC [41]. Using our fit to the NFW profile and an energy threshold of 100 MeV, the maximum flux produced by a viable SUSY model is $\simeq 3.3 \times 10^{-9}$ photons $\text{cm}^{-2} \text{s}^{-1}$, corresponding to $m_\chi \simeq 50 \text{ GeV}$ and $\langle\sigma v\rangle_\gamma \simeq 2 \times 10^{-26} \text{ cm}^3 \text{s}^{-1}$. While being consistent with the flux detected by EGRET, even the maximum predicted flux is almost two orders of magnitude too low, suggesting that the primary source is cosmic rays. Consequently, EGRET’s observations do not constrain the parameter space.

EGRET’s measurement indicates that cosmic ray induced γ -rays may be an additional background component to consider when trying to detect flux from neutralino annihilation. Following a method similar to that presented in [42], we calculate this cosmic ray induced background. We review very briefly here the basic points of the calculation and refer the reader to that study for more details. The basic assumption is that cosmic ray acceleration takes place in supernovae remnants. Working in the frame of the “leaky box model” for cosmic ray propagation, the authors calculate the expected cosmic ray flux in the LMC by considering the cosmic ray flux measured for the Milky Way and the supernova rates observed for the Milky Way and the LMC. For the γ -ray emissivity they include γ -rays from decays of neutral pions produced by proton and heavier nuclei interactions, as well as γ -rays produced via bremsstrahlung of cosmic ray electrons.

The calculation of the cosmic ray induced γ -rays in [42] focuses on the flux coming from the entire LMC. However, from an observational standpoint it is useful to examine the angular dependence of the signal. We calculate the

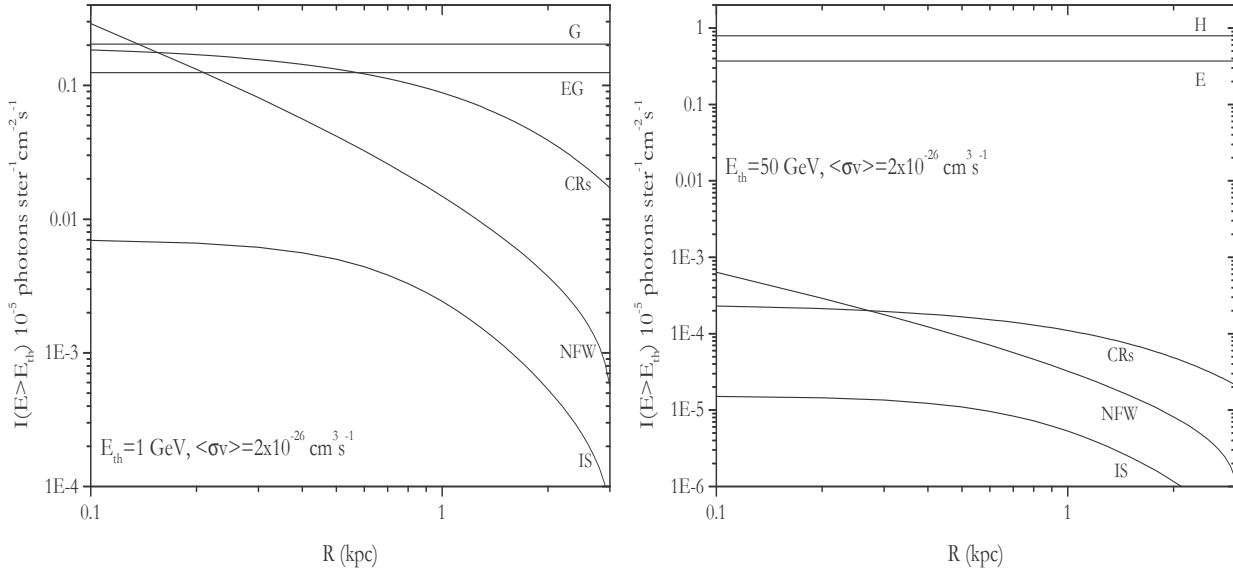


Fig. 2. *Left panel:* Specific intensity as a function of projected distance from the center of the LMC for several background contributions and the neutralino signal above 1 GeV. The signal is shown for the NFW profile and the isothermal sphere with a core (IS). The background components are labeled as follows: G for galactic, EG for extragalactic, CRs for cosmic rays. *Right panel:* Same as left panel but for an energy threshold of 50 GeV. The background components in this case are labeled as follows: H for hadronic and E for electronic.

specific intensity as a function of projected distance from the center of the LMC. To do this, it is necessary to assume a certain distribution for the HI and H₂ gas in the LMC, rather than using a mean gas surface density as in [42]. According to [26], the gas in the LMC appears to be distributed approximately as a disk with a z -scalelength of about 600 pc and the HI disk is about 7.3 kpc in diameter. Assuming an exponential distribution in R as well, we equate the 7.3 kpc to 6 radial scalelengths and obtain a scalelength of ~ 1.2 kpc, which is close to the scale length of the stellar distribution (see, e.g., [28]). Lastly, we normalize the density profile so that when integrated over the line of sight coordinate, z , and the projected radius, R , it yields a gas mass in agreement with observations. (Note that because the LMC is viewed approximately face-on, the rotation axis corresponds approximately to the line of sight direction and here we use z to describe both.)

In Figure 2 we show a comparison of the specific intensity of the different backgrounds, as well as that for the NFW profile and the isothermal sphere with a core. The left panel assumes an energy threshold of 1 GeV which is appropriate for GLAST, while the right panel assumes a 50 GeV threshold appropriate for ACTs. For GLAST the relevant backgrounds are the galactic and extragalactic diffuse emission. We use the expression found in [43] for the isotropic extragalactic background and the expression from [44] evaluated

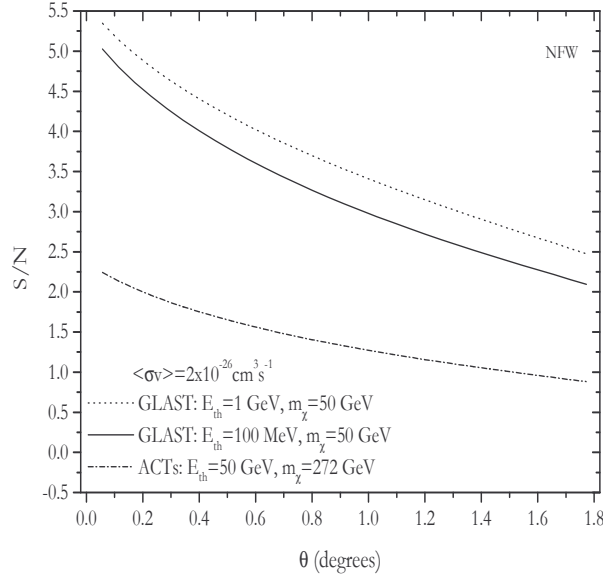


Fig. 3. Angular dependence of the signal-to-noise ratio for a NFW dark matter halo profile. For GLAST we use $A_{eff} = 10^4 \text{cm}^2$ and 1 year of observation. For ACTs we take $A_{eff} = 10^9 \text{cm}^2$ and 1 month of observation.

at the LMC galactic coordinates ($l = 280.46^\circ, b = -32.89^\circ$) for the galactic background. For ACTs the relevant backgrounds are the hadronic and electronic cosmic ray shower contributions [44,45], though it is worth noting that ACTs can reject hadronic showers with high efficiency. Clearly, the cosmic ray background is not dominant at these energy thresholds. At very low energy thresholds (100 MeV – not shown in the Figure) the cosmic ray background does become dominant in the very central regions (inner ~ 0.5 kpc). As a consistency check, after calculating the specific intensity of the cosmic ray induced flux above 100 MeV, we integrate it over solid angle and recover the $\sim 10^{-7} \text{photons cm}^{-2} \text{s}^{-1}$ prediction of [42]. This value is approximately equal to the flux measured by EGRET.

Observationally, the most relevant quantity is the signal-to-noise ratio and its angular and energy dependence. In Figure 3 we present the signal-to-noise for the flux within an angle θ , assuming the NFW profile. We show results for three different energy thresholds with the neutralino parameters for each chosen to optimize the signal. We use the specifications for each instrument as indicated. For the noise all the relevant backgrounds, including the cosmic ray induced emission, were used. From the figure it is clear that focusing on the central regions may help to achieve higher signal-to-noise ratios. As expected, for the isothermal sphere with a core (not shown here), the results are less optimistic.

Taking the idealized case of no systematic errors, the detectability condition

requires that the signal-to-noise exceed the desired significance s ,

$$\frac{F_{min} A_{eff} t}{\sqrt{N_b}} \geq s, \quad (15)$$

where F_{min} is the minimum required flux for an s - σ detection to be achieved by an instrument of effective area A_{eff} , integration time t , and number of background counts for the exposure N_b . The detectability of the neutralino induced flux for a particular SUSY model depends on the neutralino mass and the annihilation cross section for that model. The neutralino induced flux must exceed F_{min} in order to be detectable. This condition can be used to divide the m_χ - $\langle\sigma v\rangle_\gamma$ parameter space into detectable and undetectable models for each instrument. This is shown in Fig. 4. The points represent SUSY models produced using the DarkSUSY package [46]. Models with m_χ - $\langle\sigma v\rangle_\gamma$ above a given line are accessible to observation by the corresponding instrument, while models in the lower region do not yield a detectable flux.

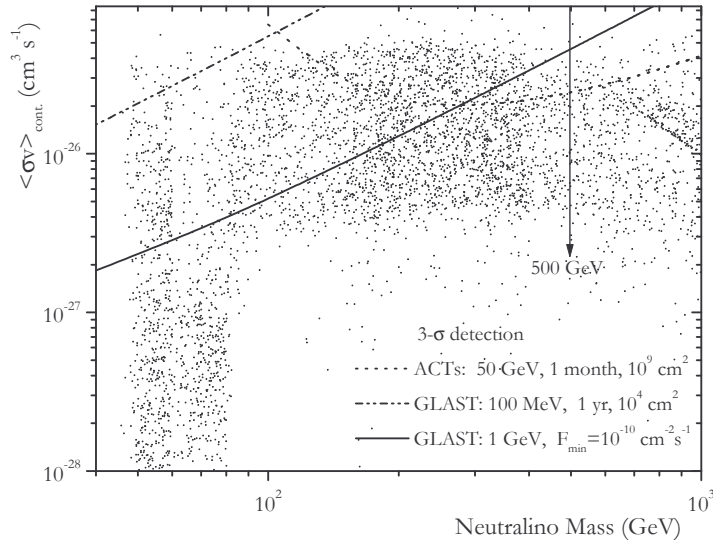


Fig. 4. The minimum detectable $\langle\sigma v\rangle_\gamma$ versus m_χ for the NFW profile. SUSY models above each curve yield a detectable signal for the instrument and observational parameters assumed. The dotted line represents observations by upcoming ACTs with 50 GeV threshold, 100 hours of observation, and 10^8 cm^2 effective area. The dashed line shows detectability by ACTs with an effective area of 10^9 cm^2 which will be achievable only at high energy thresholds ($\sim 1 \text{ TeV}$). The solid line is derived for GLAST using the expected flux sensitivity $\sim 10^{-10} \text{ cm}^{-2} \text{s}^{-1}$. The dot-dashed line is derived for GLAST for 1 year of observation, an effective area of $\sim 10^4 \text{ cm}^2$, and an energy threshold of 100 MeV.

For GLAST, the solid line is derived for the optimistic case of a flux sensitivity of $\sim 10^{-10} \text{ photons cm}^{-2} \text{s}^{-1}$, which is the expected point source flux sensitivity of GLAST for energies above $\sim 1 \text{ GeV}$ [47]. This flux sensitivity

corresponds to a $5\text{-}\sigma$ detection and 1 year of on-target observation. During normal operation, each source will only be in GLAST's field of view about 20% of the time. Consequently, the actual time required to achieve a detection of the same significance is approximately 5 times the necessary on-target time. This is within reach since the GLAST science requirement is 5 years of operation, while the lifetime goal is 10 years. If GLAST achieves its expected sensitivity, then it will be able to detect the neutralino signal for a significant portion of the parameter space. This is particularly true in light of the recently derived limit $m_\chi < 500$ GeV [4] (vertical arrow in Fig. 4). Additionally, a typical value for the total thermally averaged cross section times velocity is $\langle\sigma v\rangle_{tot} \simeq 2 \times 10^{-26} \text{ cm}^3 \text{ s}^{-1}$ (using $\Omega_m h^2 \simeq 3 \times 10^{-27} \text{ cm}^3 \text{ s}^{-1} / \langle\sigma v\rangle_{tot}$ from e.g., [2], with $\Omega_m h^2 \simeq 0.135$ [1]). By making the approximation that all neutralinos annihilate into pions, and that all neutral pions (roughly one third of all pions) annihilate to produce γ s, $\langle\sigma v\rangle_\gamma$ is about a factor of 3 smaller than $\langle\sigma v\rangle_{tot}$. Thus, a typical value for $\langle\sigma v\rangle_\gamma$ is, e.g., $\sim 7 \times 10^{-27} \text{ cm}^3 \text{ s}^{-1}$. If no annihilation signal is detected, the corresponding part of the parameter space can be ruled out.

For an energy threshold equal to 100 MeV we take $A_{eff} = 10^4 \text{ cm}^2$, 1 year of on-target observation and $\Delta\Omega_{LMC} \simeq 1.13 \times 10^{-2} \text{ sr}$ for the solid angle relevant for the collection of noise (since the LMC will be resolved by GLAST). With the sensitivity for this energy threshold only a small portion of the parameter space will be detectable (dot-dashed line in Fig. 4). Clearly, the best chance for detection is by using moderate energy thresholds, such as the 1 GeV case, for which the backgrounds are relatively low but the source photons are still numerous. To identify neutralino annihilation as the origin of the observed flux, the spectrum and its characteristic features, such as the cutoff at $E = m_\chi$, may be useful. In addition, monochromatic lines produced by neutralino annihilation (e.g., the $\gamma\gamma$ line at $E = m_\chi$) can be excellent observational signatures for a small region of parameter space where these processes are not strongly suppressed (see, e.g., [14]).

The detectability prospects for existing and upcoming ACTs are less optimistic. The commonly assumed specifications are $A_{eff} = 10^8 \text{ cm}^2$, $E_{th} = 50$ GeV and 100 hours of observation. For these specifications we find that no models will be detectable. A large integration time (~ 1 month) and effective area ($\sim 10^9 \text{ cm}^2$) (dotted line in the Figure 4) would improve the chances for detection. However, such integration times are fairly long for ACT observations and such large effective areas for an energy threshold of ~ 50 GeV are beyond the goals of existing and upcoming ACTs. Effective areas of order 10^9 cm^2 are expected to be achieved by ACTs for energies ~ 1 TeV, but the number of γ -rays produced by dark matter annihilation with energies $\gtrsim 1$ TeV is expected to be zero for models where the upper limit on $m_\chi < 500$ GeV holds.

Of the upcoming ACTs, the LMC will only be visible to HESS [48] and CAN-

GAROO III [49] due to its position in the sky. However, the zenith-angle dependence of the effective area of these instruments greatly decreases the prospects for detection. The minimum zenith angle of the LMC (at local meridian crossing) is $\sim 46^\circ$ and 39° for HESS and CANGAROO III, respectively. The energy threshold increases and the effective area is drastically reduced for these large zenith angles, requiring even longer integration times.

In this section we focused our flux calculations on the NFW fit and also discussed the less favorable case of the isothermal sphere with a core. In addition, we estimated the change in flux for other profiles. Of the range of profiles we considered, the fluxes produced vary by less than an order of magnitude, and hence the detectable cross sections and neutralino masses do not differ greatly from those of the NFW profile. This mild dependence on the detailed profile arises from our integrating to a radius R which includes most of the LMC as it appears in γ -ray observations. We find that the cosmic ray induced background is largely subdominant compared with other background sources, and that for the signal to exceed all backgrounds, observations of the central region of the LMC may be the most promising.

4 The synchrotron emission

Neutralino annihilation not only generates neutral pions, but also a comparable number of charged pions. The charged pions decay as

$$\pi^+ \rightarrow \mu^+ \nu_\mu \text{ and } \pi^- \rightarrow \mu^- \bar{\nu}_\mu. \quad (16)$$

Muons then decay via

$$\mu^+ \rightarrow e^+ \bar{\nu}_\mu \nu_e \text{ and } \mu^- \rightarrow e^- \nu_\mu \bar{\nu}_e. \quad (17)$$

In the presence of magnetic fields, the electrons and positrons produced in this way generate synchrotron radiation. The synchrotron emission from neutralino annihilation has been considered for a variety of objects including the galactic center [6], dark matter clumps [17], Draco [10], and halos of galaxy clusters [22]. Here we follow previous studies and calculate the synchrotron emission due to neutralino annihilation in the LMC.

The radio flux from the LMC has been measured in frequencies from 19.7 to 8550 MHz. The electron energies with maximum synchrotron emission in this range are relatively low (~ 20 GeV for the most energetic 8550 MHz synchrotron photons for a $5 \mu\text{G}$ magnetic field). Thus, we can consider only the dominant source of electrons and positrons for these energies: the π^\pm decays.

This is valid for gaugino-like neutralinos (see [22] and references therein). We use the analog of Eq. (6) (substituting π^0 with charged pions which we denote by π) for the charged pion spectrum, dN_π/dE_π , produced by quark fragmentation.

The number of electrons and positrons produced per annihilation per energy interval dN_e/dE_e is then given by

$$\frac{dN_e}{dE_e} = \int_{E_e}^{m_\chi c^2} \int_{E_\mu}^{aE_\mu} \frac{dN_\pi}{dE_\pi} \frac{dN_\mu^{(\pi)}}{dE_\mu} \frac{dN_e^{(\mu)}}{dE_e} dE_\pi dE_\mu, \quad (18)$$

where $a \equiv (m_\pi/m_\mu)^2$,

$$\frac{dN_\mu^{(\pi)}}{dE_\mu} = \frac{1}{E_\pi} \frac{m_\pi^2}{m_\pi^2 - m_\mu^2}, \quad (19)$$

and

$$\frac{dN_e^{(\mu)}}{dE_e} = \frac{2}{E_\mu} \left[\frac{5}{6} - \frac{3}{2} \left(\frac{E_e}{E_\mu} \right)^2 + \frac{2}{3} \left(\frac{E_e}{E_\mu} \right)^3 \right]. \quad (20)$$

Eqs. (19) and (20) give the decay products from charged pion and muon decays, respectively. For simplicity, we adopt the notation π for π^\pm and e for e^\pm .

The source spectrum q_e which is the number of electrons per unit time, volume, and energy can be written as

$$q_e = n_\chi^2 \langle \sigma v \rangle \left(\frac{dN_e}{dE_e} \right), \quad (21)$$

with $\langle \sigma v \rangle$ in this section denoting the thermally averaged cross section times velocity for annihilation into charged pions. For electron energies relevant to the frequency range that we use, the source spectrum can be altered by synchrotron losses and inverse Compton scattering (ICS) (see, e.g., [50]). The final spectrum dn_e/dE_e including losses is

$$\frac{dn_e}{dE_e} \simeq q_e \tau \quad (22)$$

where τ is the average lifetime of an electron with energy E_e ,

$$\tau \simeq \frac{E_e}{dE_e/dt}. \quad (23)$$

The dominant loss process and, thus, the shortest lifetime, is used in Eq. (22).

The total synchrotron power emitted from an electron of energy E_e , in the presence of a magnetic field $B_\mu = |\vec{B}|$ in microgauss, is [51]

$$\frac{dE_{\text{syn}}}{dt} = 1.6 \times 10^{-15} B_\mu^2 E_e^2 \text{ erg/s}. \quad (24)$$

Combining Eqs. (23) and (24) we find τ_{syn} , the time scale for energy losses due to synchrotron emission.

In order to estimate τ_{syn} one needs the local magnetic field B_μ . There are numerous estimates in the literature of the component of the magnetic field along the line of sight $B_{\mu, \text{los}}$. Rotation measure analyses of pulsars in the LMC indicate a $B_{\mu, \text{los}}$ ranging from ~ 0.4 to $5 \mu G$ [52,53]. Similar values ($B_{\mu, \text{los}} \simeq 2 \mu G$) were obtained from the polarized radio continuum emission [54]. Estimates of the total magnetic field, rather than the component of the magnetic field along the line of sight, are more indirect and typically involve more assumptions. Several studies seem to converge to $\sim 6 \mu G$ [55,56], while the largest value estimated for the total magnetic field is $\simeq 18.4 \mu G$ [57]. In what follows we adopt the value of $\simeq 5 \mu G$ for the total magnetic field, unless otherwise specified.

For magnetic fields of $5 \mu G$, synchrotron losses dominate over ICS processes off the cosmic microwave background, the optical photons, and the produced synchrotron photons themselves. Therefore, the relevant timescale in Eq. (22) is τ_{syn} .

The synchrotron emission coefficient j_ν (number of photons of frequency ν emitted per unit time, volume, and frequency) is

$$j_\nu = \frac{dn_e}{dE_e} \frac{dE_e}{d\nu} \frac{dE_{\text{syn}}}{dt} \frac{\text{erg}}{\text{cm}^3 \text{s Hz}}. \quad (25)$$

To calculate the factor $dE_e/d\nu$ appearing in the expression for the emission coefficient, we use the relation between E_e and the frequency where maximum synchrotron emission occurs for this electron energy. The frequency of maximum synchrotron emission is equal to $\simeq 0.29\nu_c$, with the cutoff frequency $\nu_c = 3/2\gamma^3\nu_B$ where γ is the Lorentz factor and $\nu_B = (eB \sin \alpha / 2\pi\gamma mc)$ is the relativistic gyrofrequency. Taking the power weighted average over the pitch

angle α , the frequency of maximum emission is

$$\nu_{\max} = 4.1 B_{\mu} \left(\frac{E_e}{\text{GeV}} \right)^2 \text{ MHz} . \quad (26)$$

Using Eqs. (18), (21), (22), (23), (24), and (26) to calculate j_{ν} from Eq. (25), and substituting the latter in Eq. (12) we calculate the synchrotron flux. For the integration we use the same R that we use in the γ -rays since the extent of the LMC in the two frequency ranges is similar [40].

The synchrotron flux F_{syn} in Jy ($1 \text{ Jy} = 10^{-23} \text{ ergs cm}^{-2} \text{ s}^{-1} \text{ Hz}^{-1}$) is

$$F_{syn} \simeq 3.1 \times 10^{10} \frac{\langle \sigma v \rangle}{m_{\chi}^2} \frac{dN_e}{dE_e} \frac{K}{B_{\mu}} \text{ Jy} , \quad (27)$$

where K is given by Eq. (13) and is in units of $(\text{GeV}/c^2)^2 \text{ cm}^{-5}$. Again, the neutralino mass m_{χ} is given in GeV and $\langle \sigma v \rangle$ in $\text{cm}^3 \text{ s}^{-1}$. The frequency dependence of the flux is given by

$$\frac{dN_e}{dE_e} \propto 2.48 - 1.22x^{-0.5} + 0.22x^2 + 0.10x^{-1.5} - 1.54x^{0.5} - 0.04x^3 , \quad (28)$$

where $x = E_e/m_{\chi}c^2 \simeq (4.94 \times 10^{-4} B_{\mu}^{-0.5} \nu^{0.5}/m_{\chi})$, with ν in Hz and m_{χ} in GeV. The dependence on ν varies with the electron energy and the neutralino mass and goes as $\nu^{-0.75}$ at sufficiently small energies.

A compilation of radio observations of the LMC from 1959 to 1991 in the frequency range (19.7 – 8550) MHz is presented along with the corresponding references in [56]. As can be seen in Fig. 5, the observed LMC spectrum in the (19.7 – 8550) MHz range has a steep contribution from synchrotron radiation which dominates at lower frequencies until around 2×10^3 MHz, at which point the thermal emission becomes dominant. A least squares fit of the form $S_{\nu} = S_{0,th} \nu^{-0.1} + S_{0,nth} \nu^{-\alpha_{nth}}$ to the data yields a total flux density at 1 GHz of 610 ± 10 Jy, a non-thermal spectrum with $\alpha_{nth} = 0.70 \pm 0.06$, and a fraction of thermal emission at 1 GHz of $(45 \pm 10)\%$ [56]. Using this information we find $S_{0,th} \simeq 2.2 \times 10^3$ and $S_{0,nth} \simeq 6.7 \times 10^8$. The data points and the decomposition into thermal and non-thermal emission are shown in Fig. 5. We also plot F_{syn} for $m_{\chi} = 50$ GeV and $\langle \sigma v \rangle = 2.2 \times 10^{-26} \text{ cm}^3 \text{ s}^{-1}$, for the NFW dark matter profile. The thick solid line corresponds to $B_{\mu} = 5 \mu G$; the lighter line represents the results for the maximum total magnetic field estimated in literature ($18.4 \mu G$ [57]).

In the more realistic case of $B_{\mu} = 5 \mu G$, neutralino-induced synchrotron emission clearly may be part of the observed flux, but is lower than the total

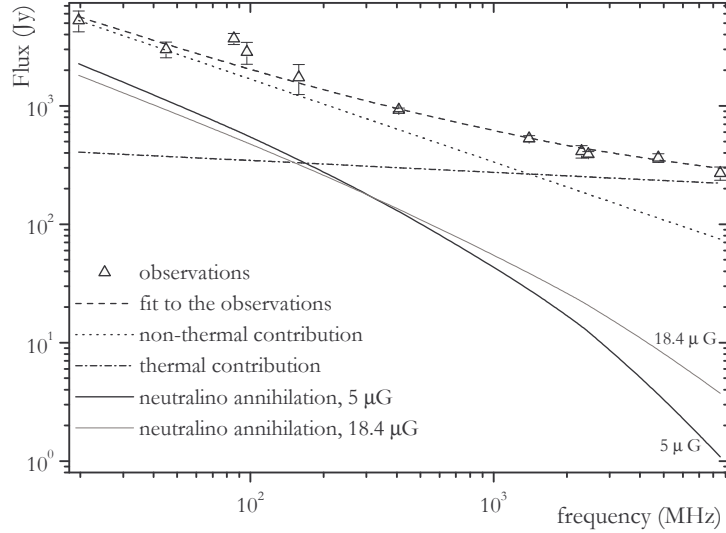


Fig. 5. The flux in Jy as a function of frequency in the range from 19.7 to 8550 MHz. The open triangles correspond to LMC data taken over the period from 1959 to 1991; the dashed line is a best fit to the data assuming a decomposition into thermal and non-thermal emission. The dotted line corresponds to the non-thermal contribution, and the dot-dashed line to the thermal contribution. The flux from neutralino annihilation for $m_\chi = 50$ GeV, $B_\mu = 5 \mu G$, and $\langle\sigma v\rangle \simeq 2 \times 10^{-26} \text{ cm}^3 \text{ s}^{-1}$, is given by the thick solid line. The remaining line corresponds to $B_\mu = 18.4 \mu G$, which is the maximum published estimate for the total magnetic field (see text for details). The $B_\mu \simeq 5 \mu G$ case is the most realistic value, even though the results in these frequencies do not change dramatically even when a $18.4 \mu G$ field is used.

observed flux, especially at higher frequencies. In the low frequency region, the signal increases enough to exceed the thermal contribution to the observation. Given that the neutralino signal ($\propto \nu^{-0.75}$) is almost parallel to the non-thermal component ($\propto \nu^{-0.70}$), even at reasonably low radio frequencies the neutralino flux is sub-dominant. A mildly constraining limit on neutralino cross-sections can be reached by requiring that F_{syn} be less than or equal to the non-thermal contribution in S_ν at low frequencies. The frequency dependence essentially drops out and we find $\langle\sigma v\rangle \leq 1.24 \times 10^{-9} m_\chi^{1.5} B_\mu^{0.25} / K$. Thus, assuming the NFW fit and $m_\chi = 50$ GeV, any $\langle\sigma v\rangle$ lower than $\sim 2 \times 10^{-26} \text{ cm}^3 \text{ s}^{-1}$ gives a flux at low frequencies consistent with observation. The allowed $\langle\sigma v\rangle$ become even larger at larger neutralino masses. Thus, the observations do not put severe constraints on the allowed cross sections. Although we have focused on the NFW profile, the synchrotron fluxes vary slightly depending on the halo profile used, as discussed in §III.

The best hope for distinguishing the synchrotron emission generated by cosmic rays from that produced by neutralino annihilation is to use the fact that the density profile of cosmic rays differs from the dark matter density profile. While the dark matter halo extends significantly beyond the disk, the density

of cosmic rays is expected to rapidly decrease at large radii. If low radio frequency observations of the LMC are made with high angular resolution, the change from cosmic ray to neutralino dominance should be apparent as one moves away from the LMC disk. Currently there is no telescope that could carry out observations of the LMC at frequencies less than about 20 MHz. Such low frequencies are extremely difficult to observe from the ground due to ionospheric absorption and scattering. One promising ground-based project is the Low Frequency Array (LOFAR) [58] which should reach frequencies down to ~ 10 MHz and a flux sensitivity of a few mJy in 1 hour. However, the site of the instrument has not yet been decided, so the LMC may not necessarily be observable. To reach even lower frequencies, where ionospheric absorption is very intense, space-based instruments are required. The proposed Astronomical Low Frequency Array (ALFA) [59] should reach down to ~ 0.3 MHz.

5 Discussion and conclusions

We have studied the γ -ray and synchrotron emission from neutralino annihilation in the LMC. We modeled the dark matter profile of the LMC by fitting modern profiles found in N-body simulations to rotation velocity data. Although we focused on the NFW best fit density profile when deriving our γ -ray and synchrotron fluxes, we also considered a less concentrated dark matter profile (the isothermal sphere with a core) and a more concentrated one (the Moore et al. profile). This range of profiles changes our results by less than an order of magnitude for the same rotation curve. If one takes into account the expected compression of the dark matter due to baryons, which would cause even a shallow, core-dominated dark matter distribution to become cuspy, it is reasonable to assume that the actual fluxes may be several orders of magnitude greater. Prada et al. [33] found that baryonic compression can enhance the central density by more than an order of magnitude.

The LMC rotation curve data has been recently re-analyzed by van der Marel et al. [23] who claim that the plateau value for the rotation velocity is not $\sim (60-70)$ km/s as found in most studies, but ~ 50 km/s. Their conclusion is based on a re-analysis of carbon star data including corrections for the transverse motion of the LMC, as well as for nutation and precession effects. Their resulting rotation curve has large errors and is sparse at small radii, but a fit to their rotation curve results in K up to ~ 1 order of magnitude less than those we found using the initial data. The quality of the fits is much poorer given the sparseness at small radii.

An additional uncertainty is introduced by the fact that only the line-of-sight component of the velocity can be observed. The assumptions necessary to re-

cover the total velocity from the line-of-sight component may result in an over- or underestimation of the actual velocity, thereby improving or worsening the prospects for detection.

The predicted cosmic ray induced γ -ray and synchrotron emission appears to be of similar magnitude to the observed emission. A high angular resolution study of both neutralino and cosmic ray induced emission from the LMC may be key to utilizing the closest known dark matter “clump” as a laboratory for testing neutralino parameters. Smaller solid angles help reduce the collection of noise, and, most importantly, a study of the spatial dependence of the emission can help GLAST and radio observations distinguish between neutralino and cosmic ray produced signals.

Summarizing, we find that neither the EGRET measurement of γ -rays above 100 MeV from the LMC nor the low frequency synchrotron observations significantly constrain the SUSY parameter space. The maximum γ -ray flux for the considered profiles is almost ~ 2 orders of magnitude less than the observed flux, whereas all models with $\langle\sigma v\rangle \lesssim 2 \times 10^{-26} \text{ cm}^3 \text{ s}^{-1}$ are consistent with the observed synchrotron flux. Existing and upcoming ACTs will not be able to probe the SUSY parameter space, unless the neutralino profiles are more centrally concentrated or observers use longer integration times and larger effective areas larger than currently planned. Since the sensitivity becomes better for a larger exposure (effective area \times integration time), the problem of a small effective area may be compensated for by larger integration times. However, these integration times may not be realistic. Added to these difficulties, the location of the LMC makes it difficult to observe even for some instruments in the southern hemisphere.

GLAST on the other hand, being a satellite, will not find the LMC location problematic. If systematic errors are small, GLAST will be able to probe a significant part of the allowed parameter space, especially if the recent limit $m_\chi < 500 \text{ GeV}$ is taken into account. The comparison of the γ -ray annihilation signal to the EGRET measurement implies that there is another dominant source of this flux, most likely cosmic rays. The synchrotron study finds this result as well. Thus, the spectral features of the neutralino annihilation signal, in particular the shape and cutoff of the spectrum at m_χ , will be essential to disentangle the neutralino signal.

The synchrotron signal is at best a factor of ~ 3 less than the observed signal, with this discrepancy increasing with increasing frequency. The flux values for the frequency range we use vary from ~ 1 to $\sim 1000 \text{ Jy}$, easily detectable levels. The difficulty will again be in disentangling the neutralino induced signal from the total flux. At low frequencies, the frequency dependence of the calculated flux is almost identical to that of the observed spectrum. The best hope for observing the synchrotron emission due to neutralino annihilation is

a high angular resolution study at low frequencies which may be possible with proposed observatories such as LOFAR or ALFA.

Acknowledgements

This work was supported in part by the NSF through grant AST-0071235 and DOEgrant DE-FG0291-ER40606 at the University of Chicago and at the Center for Cosmological Physics by grant NSF PHY-0114422. A.O. thanks the Aspen Center for Physics for its hospitality while this work was completed.

References

- [1] D. N. Spergel, L. Verde, H. V. Peiris, E. Komatsu, M. R.olta, C. L. Bennett, M. Halpern, G. Hinshaw, N. Jarosik, A. Kogut, M. Limon, S. S. Meyer, L. Page, G. S. Tucker, J. L. Weiland, E. Wollack, E. L. Wright, astro-ph/0302209.
- [2] G. Jungman, M. Kamionkowski, K. Griest, Phys. Rep. 267 (1996) 195.
- [3] J. Ellis, J. S. Hagelin, D. V. Nanopoulos, K. Olive, M. Srednicki, Nuclear Physics B 238 (1984) 453.
- [4] J. Ellis, K. A. Olive, Y. Santoso, V. C. Spanos, hep-ph/0303043.
- [5] K. Hagiwara, et al., Phys. Rev. D 66 (2002) 10001.
- [6] V. Berezhinsky, A. Gurevich, K. Zybin, Phys. Rev. Lett. B 294 (1992) 221.
- [7] P. Gondolo, J. Silk, Phys. Rev. Lett. 83 (1999) 1719.
- [8] A. Cesarini, F. Fucito, A. Lionetto, A. Morselli, P. Ullio, astro-ph/0305075.
- [9] E. A. Baltz, C. Briot, P. Salati, R. Taillet, J. Silk, Phys. Rev. D 61 (2000) 23514.
- [10] C. Tyler, Phys. Rev. D 66 (2002) 23509.
- [11] V. V. Vassiliev, astro-ph/0305584.
- [12] L. Bergström, J. Edsjö, P. Gondolo, P. Ullio, Phys. Rev. D 59 (1999) 43506.
- [13] C. Calcáneo-Roldán, B. Moore, Phys. Rev. D 62 (2000) 123005.
- [14] A. Tasitsiomi, A. V. Olinto, Phys. Rev. D 66 (2002) 83006.
- [15] P. Ullio, L. Bergström, J. Edsjö, C. Lacey, Phys. Rev. D 66 (2002) 123502.
- [16] V. Berezhinsky, V. Dokuchaev, Y. Eroshenko, astro-ph/0301551.
- [17] P. Blasi, A. V. Olinto, C. Tyler, Astropart. Phys. 18 (2003) 649.

- [18] J. E. Taylor, J. Silk, *Mon. Not. R. Astron. Soc.* 339 (2003) 505.
- [19] P. Gondolo, *Nucl. Phys. Proc. Suppl.* 35 (1994) 148.
- [20] A. Falvard, E. Giraud, A. Jacholkowska, J. Lavalle, E. Nuss, F. Piron, M. Sapinski, P. Salati, R. Taillet, K. Jedamzik, G. Moulaka, *astro-ph/0210184*.
- [21] E. Giraud, G. Meylan, M. Sapinski, A. Falvard, A. Jacholkowska, K. Jedamzik, J. Lavalle, E. Nuss, G. Moulaka, F. Piron, P. Salati, R. Taillet, *astro-ph/0209230*.
- [22] S. Colafrancesco, B. Mele, *Astrophys. J.* 562 (2001) 24.
- [23] R. P. van der Marel, D. R. Alves, E. Hardy, N. B. Suntzeff, *Astron. J.* 124 (2002) 2639.
- [24] S. J. Meatheringham, M. A. Dopita, H. C. Ford, B. L. Webster, *Astrophys. J.* 327 (1988) 651.
- [25] R. A. Schommer, N. B. Suntzeff, E. W. Olszewski, H. C. Harris, *Astron. J.* 103 (1992) 447.
- [26] S. Kim, L. Staveley-Smith, M. A. Dopita, K. C. Freeman, R. J. Sault, M. J. Kesteven, D. McConnell, *Astrophys. J.* 503 (1998) 674.
- [27] Y. Sofue, *Pub. Astron. Soc. Jap.* 51 (1999) 445.
- [28] D. R. Alves, C. A. Nelson, *Astrophys. J.* 542 (2000) 789.
- [29] J. F. Navarro, C. S. Frenk, S. D. M. White, *Mon. Not. R. Astron. Soc.* 275 (1995) 720.
- [30] J. F. Navarro, C. S. Frenk, S. D. White, *Astrophys. J.* 462 (1996) 563.
- [31] B. Moore, F. Governato, T. Quinn, J. Stadel, G. Lake, *Astrophys. J.* 499 (1998) L5.
- [32] A. Tasitsiomi, *Int. J. Mod. Phys. D* 12 (2003) 1157.
- [33] F. Prada, A. Klypin, J. Flix, M. Martinez, E. Simonneau, *Astrophysical inputs on the SUSY dark matter annihilation detectability*, *ArXiv Astrophysics e-prints*.
- [34] E. Hayashi, J. F. Navarro, J. E. Taylor, J. Stadel, T. Quinn, *Astrophys. J.* 584 (2003) 541.
- [35] A. V. Kravtsov, private communication.
- [36] A. Klypin, S. Gottlöber, A. V. Kravtsov, A. M. Khokhlov, *Astrophys. J.* 516 (1999) 530.
- [37] F. Stoeckl, S. D. M. White, G. Tormen, V. Springel, *Mon. Not. R. Astron. Soc.* 335 (2002) L84.
- [38] C. T. Hill, *Nucl. Phys. B* 224 (1983) 469.

- [39] L. Bergström, J. Edsjö, P. Ullio, *Phys. Rev. Lett.* 87 (2001) 251301.
- [40] P. Sreekumar, D. L. Bertsch, B. L. Dingus, C. E. Fichtel, R. C. Hartman, S. D. Hunter, G. Kanbach, D. A. Kniffen, Y. C. Lin, J. R. Mattox, H. A. Mayer-Hasselwander, P. F. Michelson, C. von Montigny, P. L. Nolan, K. Pinkau, E. J. Schneid, D. J. Thompson, *Astrophys. J. Lett.* 400 (1992) L67.
- [41] R. C. Hartman, et al., *Astrophys. J. Suppl. Ser.* 123 (1999) 79.
- [42] V. Pavlidou, B. D. Fields, *Diffuse Gamma Rays from Local Group Galaxies*, *Astrophys. J.* 558 (2001) 63–71.
- [43] P. Sreekumar, D. L. Bertsch, B. L. Dingus, J. A. Esposito, C. E. Fichtel, R. C. Hartman, S. D. Hunter, G. Kanbach, D. A. Kniffen, Y. C. Lin, H. A. Mayer-Hasselwander, P. F. Michelson, C. von Montigny, A. Muecke, R. Mukherjee, P. L. Nolan, M. Pohl, O. Reimer, E. Schneid, J. G. Stacy, F. W. Stecker, D. J. Thompson, T. D. Willis, *Astrophys. J.* 494 (1998) 523.
- [44] L. Bergström, P. Ullio, J. H. Buckley, *Astropart. Phys.* 9 (1998) 137.
- [45] M. Longair, *High Energy Astrophysics*, Cambridge University Press, Cambridge, England, 1992.
- [46] P. Gondolo, J. Edsjo, P. Ullio, L. Bergstrom, M. Schelke, E. A. Baltz, *astro-ph/0211238*.
- [47] A. de Angelis, *astro-ph/0009271*.
- [48] W. Hofmann, The Hess Collaboration, The High Energy Stereoscopic System (HESS) Project, in: *GeV-TeV Gamma Ray Astrophysics Workshop : towards a major atmospheric Cherenkov detector*, 2000, p. 500.
- [49] M. Mori, et al., The CANGAROO-III Project, in: *GeV-TeV Gamma Ray Astrophysics Workshop : towards a major atmospheric Cherenkov detector*, 2000, p. 485.
- [50] P. Blasi, S. Colafrancesco, *Astropart. Phys.* 12 (1999) 169.
- [51] G. Rybicki, A. Lightman, *Radiative Processes in Astrophysics*, Wiley, New York, 1979.
- [52] M. E. Costa, P. M. McCulloch, P. A. Hamilton, The Magnetic Field Strength in the Large Magellanic Cloud, in: *IAU Symp. 148: The Magellanic Clouds*, 1991, p. 101.
- [53] M. E. Costa, P. M. McCulloch, P. A. Hamilton, *Mon. Not. R. Astron. Soc.* 252 (1991) 13.
- [54] U. Klein, R. F. Haynes, R. Wielebinski, D. Meinert, *Astron. Astrophys.* 271 (1993) 402.
- [55] U. Klein, R. Wielebinski, R. F. Haynes, D. F. Malin, *Astron. Astrophys.* 211 (1989) 280.

- [56] R. F. Haynes, U. Klein, S. R. Wayte, R. Wielebinski, J. D. Murray, E. Bajaja, D. Meinert, U. R. Buczilowski, J. I. Harnett, A. J. Hunt, R. Wark, L. Sciacca, *Astron. Astrophys.* 252 (1991) 475.
- [57] X. Chi, A. W. Wolfendale, *Nature* 362 (1993) 610.
- [58] H. Rottgering, A. G. de Bruyn, R. P. Fender, J. Kuijpers, M. P. van Haarlem, M. Johnston-Hollitt, G. K. Miley, *astro-ph/0307240*.
- [59] D. L. Jones, et al., *Advances in Space Research* 26 (2000) 743.